X-ray Spectroscopy of Enzyme Active Site Analogues and Related Molecules: Bis(dithiolene)molybdenum(IV) and -tungsten(IV,VI) Complexes with Variant Terminal Ligands

Kristin B. Musgrave,[†] Booyong S. Lim,[‡] Kie-Moon Sung,[‡] R. H. Holm,*[,‡] Britt Hedman,*[,†,§] and Keith O. Hodgson*[,†,§]

Department of Chemistry, Stanford University, Stanford, California 94305, Stanford Synchrotron Radiation Laboratory, SLAC, Stanford University, Stanford, California 94309, and Department of Chemistry and Chemical Biology, Harvard University, Cambridge, Massachusetts 02138

Received June 6, 2000

The X-ray absorption spectra at the molybdenum and selenium K-edges and the tungsten $L_{2,3}$-edges are acquired for a set of 14 Mo(IV) and W(IV,VI) bis(dithiolene) complexes related to the active sites of molybdo- and tungstoenzymes. The set includes square pyramidal $[Mo^{IV}L(S_2C_2Me_2)_2]^-$ ($L = O^{2-}$, R_3SiO^-, RO^-, RS^-, RSe^-) and $[W^{IV}(OR)(S_2C_2Me_2)_2]^-$, distorted trigonal prismatic $[Mo^{IV}(CO)(SeR)(S_2C_2Me_2)_2]^-$ and $[W^{IV}(CO)L(S_2C_2Me_2)_2]^-$ ($L = RS^-$, RSe^-), and distorted octahedral $[W^{VI}O(OR)(S_2C_2Me_2)_2]^-$. The dithiolene simulates the pterin−dithiolene cofactor ligand, and L represents a protein ligand. Bond lengths are determined by EXAFS analysis using the GNXAS protocol. Normalized edge spectra, non-phase-shift-corrected Fourier transforms, and EXAFS data and fits are presented. Bond lengths determined by EXAFS and X-ray crystallography agree to ≤0.02 Å as do the M−Se distances determined by both metal and selenium EXAFS. The complexes $[Mo^{IV}(QR)(S_2C_2Me_2)_2]^-$ simulate protein ligation by the DMSO reductase family of enzymes, including DMSO reductase itself (Q = O), dissimilatory nitrate reductase (Q = S), and formate dehydrogenase (Q = Se). Edge shifts of these complexes correlate with the ligand electronegativities. Terminal ligand binding is clearly distinguished in the presence of four Mo−S(dithiolene) interactions. Similarly, five-coordinate $[ML(S_2C_2Me_2)_2]^-$ and six-coordinate $[M(CO)L(S_2C_2Me_2)_2]^-$ are distinguishable by edge and EXAFS spectra. This study expands a previous XAS investigation of bis(dithiolene)-metal(IV,V,VI) complexes (Musgrave, K. B.; Donahue, J. P.; Lorber, C.; Holm, R. H.; Hedman, B.; Hodgson, K. O. *J. Am. Chem. Soc.* **1999**, *121*, 10297) by including a larger inventory of molecules with variant physiologically relevant terminal ligation. The previous and present XAS results should prove useful in characterizing and refining metric features and structures of enzyme sites.

Introduction

Recent research in these laboratories has been directed toward the development of structural and functional analogues of the active sites of molybdo-[1−3] and tungstoenzymes.[4] These sites contain a single metal atom coordinated by one or two pterin−dithiolene cofactor ligands as shown in Figure 1, with additional coordination by protein side chains and/or exogenous ligands. In the initial phase of this work, we have concentrated on the sites present in the DMSO reductase (DMSOR) family of enzymes as defined under the Hille classification.[1] Protein crystallography and X-ray absorption spectroscopy (XAS) have afforded the structures of the oxidized (Mo^{VI}) and reduced (Mo^{IV}) sites of DMSOR,[5−8] dissimilatory nitrate reductase,[9] and formate dehydrogenase[10,11] depicted in Figure 1. The structure of the oxidized site of the DMSOR of *Rhodobacter sphaeroides* is that recently obtained by Schindelin and co-workers[6] at 1.3 Å resolution. While the matter has not been clarified, this structure may also apply to the DMSOR of *Rhodobacter capsulatus* for which seven-coordinate Mo^{VI} and six-coordinate Mo^{IV} sites have been deduced from crystallography[12,13] and XAS.[14] Structures obtained from EXAFS[11,15] for certain forms

[†] Stanford University.
[‡] Harvard University.
[§] Stanford Synchrotron Radiation Laboratory.

(1) Hille, R. *Chem. Rev.* **1996**, *96*, 2757.
(2) Romão, M. J.; Knäblein, J.; Huber, R.; Moura, J. J. G. *Prog. Mol. Biophys. Mol. Biol.* **1997**, *68*, 121.
(3) Kisker, C.; Schindelin, H.; Rees, D. C. *Annu. Rev. Biochem.* **1997**, *66*, 233.
(4) Johnson, M. K.; Rees, D. C.; Adams, M. W. W. *Chem. Rev.* **1996**, *96*, 2817.
(5) Schindelin, H.; Kisker, C.; Hilton, J.; Rajagopalan, K. V.; Rees, D. C. *Science* **1996**, *272*, 1615.
(6) Li, H.-K.; Temple, C.; Rajagopalan, K. V.; Schindelin, H. *J. Am. Chem. Soc.* **2000**, *122*, 7673.
(7) George, G. N.; Hilton, J.; Rajagopalan, K. V. *J. Am. Chem. Soc.* **1996**, *118*, 1113.
(8) George, G. N.; Hilton, J.; Temple, C.; Prince, R. C.; Rajagopalan, K. V. *J. Am. Chem. Soc.* **1999**, *121*, 1256.
(9) Dias, J. M.; Than, M. E.; Humm, A.; Huber, R.; Bourenkov, G. P.; Bartunik, H. D.; Bursakov, S.; Calvete, J.; Caldeira, J.; Carneiro, C.; Moura, J. J. G.; Moura, I.; Romão, M. J. *Structure* **1999**, *7*, 65.
(10) Boyington, J. C.; Gladyshev, V. N.; Khangulov, S. V.; Stadtman, T. C.; Sun, P. D. *Science* **1997**, *275*, 1305.
(11) George, G. N.; Colangelo, C. M.; Dong, J.; Scott, R. A.; Khangulov, S. V.; Gladyshev, V. N.; Stadtman, T. C. *J. Am. Chem. Soc.* **1998**, *120*, 1267.
(12) McAlpine, A. S.; McEwan, A. G.; Shaw, A. L.; Bailey, S. *J. Biol. Inorg. Chem.* **1997**, *2*, 690.
(13) McAlpine, A. S.; McEwan, A. G.; Bailey, S. *J. Mol. Biol.* **1998**, *275*, 613.
(14) Baugh, P. E.; Garner, C. D.; Charnock, J. M.; Collison, D.; Davies, E. S.; McAlpine, A. S.; Bailey, S.; Lane, I.; Hanson, G. R.; McEwan, A. G. *J. Biol. Inorg. Chem.* **1997**, *2*, 634.
(15) George, G. N.; Costa, C.; Moura, J. J. G.; Moura, I. *J. Am. Chem. Soc.* **1999**, *121*, 2625.

10.1021/ic000601r CCC: $19.00
Published on Web 10/26/2000

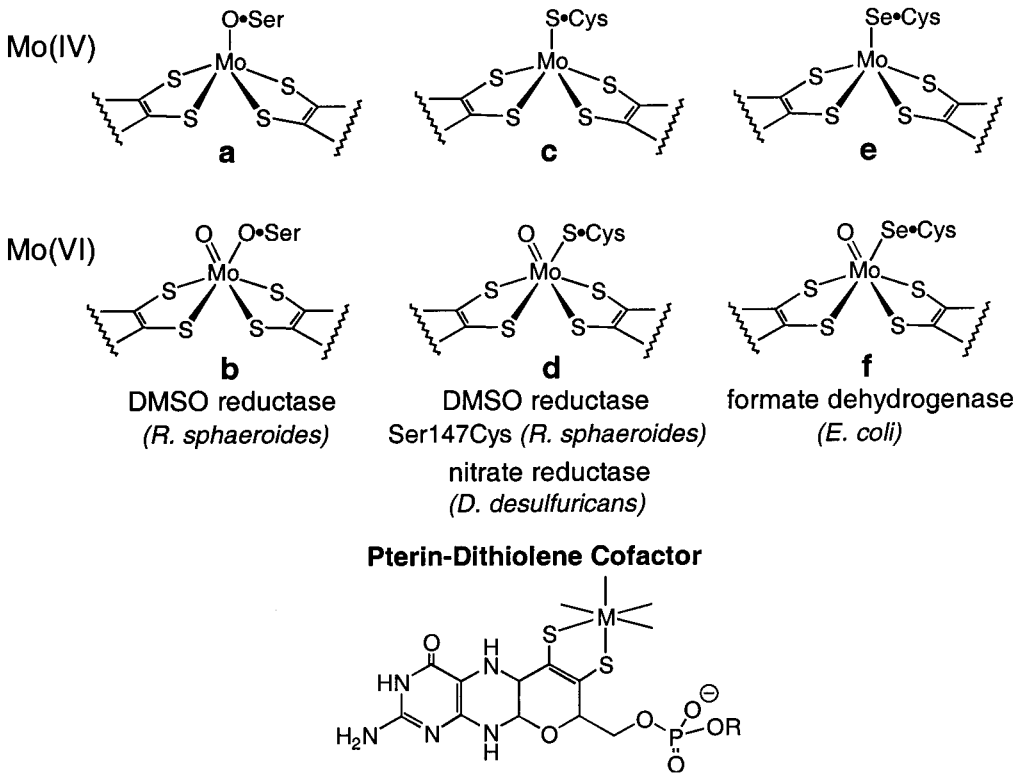

Figure 1. Schematic structures of the reduced and oxidized sites of members of the DMSO reductase enzyme family. The oxo ligand may be protonated under certain conditions. Also shown is the symmetrical binding of the pterin−dithiolene cofactor ligand (R is absent or is a nucleotide) to an M = Mo or W atom.

of formate dehydrogenase involving selenosulfide−thiolate ligands are not included in Figure 1, which contains those sites for which analogues have been sought by synthesis. Much less is known about the catalytic sites of tungstoenzymes. Two enzymes examined crystallographically, aldehyde ferredoxin oxidoreductase[16] and formaldehyde ferredoxin oxidoreductase[17] (both from *Pyrococcus furiosus*), contain two pterin−dithiolene ligands and one or two unidentified oxygenous ligands.

We have reported the syntheses and structures of complexes of the types $[Mo^{IV}O(bdt)_2]^{2-}$, $[Mo^{IV}(OSiR_3)(bdt)_2]^-$, $[Mo^{V}O(bdt)_2]^-$, and $[Mo^{VI}O(OSiR_3)(bdt)_2]^-$ (bdt = benzene-1,2-dithiolate).[18] Here bdt and silyloxide are intended to simulate pterin−dithiolene symmetrical chelation and serinate binding, respectively, in the enzymes. In the course of this and more recent work, we have prepared where possible the corresponding tungsten complexes[19] in the event that their coordination units appear in enzymes. More recently, we have incorporated the dimethyldithiolene ligand in analogue complexes of molybdenum[20] and tungsten[21,22] to provide an electronically more realistic coordination environment and to improve[23] the rather sluggish oxo transfer reactivity of bdt complexes with biological and other substrates.[18,19] The methods of synthesis allow the inclusion of a variety of terminal (non-dithiolene) ligands which encompass those indicated in Figure 1. We have reported a detailed XAS study of molybdenum and tungsten bdt complexes of the foregoing types.[24] Here we describe the results of a similar study at the molybdenum K-edge and the tungsten $L_{2,3}$-edges for the Mo^{IV} complexes **1**−**8** and the $W^{IV,VI}$ complexes **9**−**14**, whose structures are schematically depicted in Figures 2 and 3, respectively. Also reported are results obtained at the selenium K-edge. As in our previous study,[24] the principal purpose is to provide edge and EXAFS data that will prove useful in characterizing oxidation states in and structures of enzyme sites that resemble those of fully characterized analogue complexes. In the sections which follow, complexes are designated numerically according to Chart 1.

Experimental Section

Preparation of Compounds. Compounds containing complexes **1** and **3**−**14** were prepared by methods described in the references cited in Chart 1.

$(Et_4N)[Mo(OSiPh_2Bu^t)(S_2C_2Me_2)_2]$. An orange-brown solution of 94 mg (0.15 mmol) of $(Et_4N)_2[MoO(S_2C_2Me_2)_2]$[20] in 5 mL of acetonitrile was treated with 38 μL (0.15 mmol) of Bu^tPh_2SiCl. The reaction mixture was stirred for 3 h, generating a dark brown solution. The solvent was removed in vacuo, and the brown residue was dissolved in a minimal volume of acetonitrile/THF (1:5 v/v). The solution was filtered, the filtrate was taken to dryness, and the residue was dissolved in a minimal volume of acetonitrile. Several volume equivalents of ether were introduced by vapor diffusion over 2 d. The product was isolated by decanting the supernatant, washing with ether, and drying in vacuo to afford the product as 78 mg (70%) of dark brown microcrystals. UV−vis (acetonitrile): λ_{max} (ϵ_M) 341 (14 900), 393 (4520), 465 (1740), 553 (533), 655 nm (sh, 244). ^{1}H NMR (CD_3CN, anion): δ 0.76 (s, 9), 2.48 (s, 12), 7.25 (m, 2), 7.31 (m, 1), 7.46 (m, 2). Anal.

(16) Chan, M. K.; Mukund, S.; Kletzin, A.; Adams, M. W. W.; Rees, D. C. *Science* **1995**, *267*, 1463.
(17) Hu, Y.; Faham, S.; Roy, R.; Adams, M. W. W.; Rees, D. C. *J. Mol. Biol.* **1999**, *286*, 899.
(18) Donahue, J. P.; Goldsmith, C. R.; Nadiminti, U.; Holm, R. H. *J. Am. Chem. Soc.* **1998**, *120*, 12869.
(19) Lorber, C.; Donahue, J. P.; Goddard, C. A.; Nordlander, E.; Holm, R. H. *J. Am. Chem. Soc.* **1998**, *120*, 8102.
(20) Lim, B. S.; Donahue, J. P.; Holm, R. H. *Inorg. Chem.* **2000**, *39*, 263.
(21) Goddard, C. A.; Holm, R. H. *Inorg. Chem.* **1999**, *38*, 5389.
(22) Sung, K.-M.; Holm, R. H. *Inorg. Chem.* **2000**, *39*, 1275.
(23) Lim, B. S.; Sung, K.-M.; Holm, R. H. *J. Am. Chem. Soc.* **2000**, *122*, 7410.
(24) Musgrave, K. B.; Donahue, J. P.; Lorber, C.; Holm, R. H.; Hedman, B.; Hodgson, K. O. *J. Am. Chem. Soc.* **1999**, *121*, 10297.

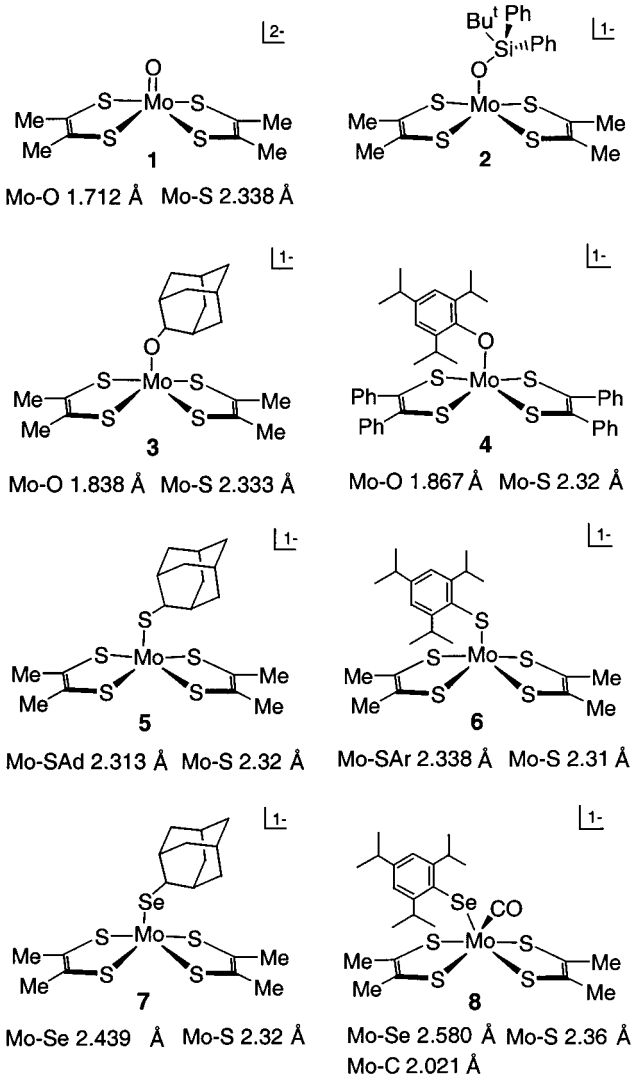

Figure 2. Schematic structures and selected mean bond lengths of bis(dithiolene)molybdenum complexes as determined by X-ray crystallography for complexes **1** and **3**−**8**. The crystal structure for **2** is not known, and this structure is based on the EXAFS determination in the current paper, with distances given in Table 1.

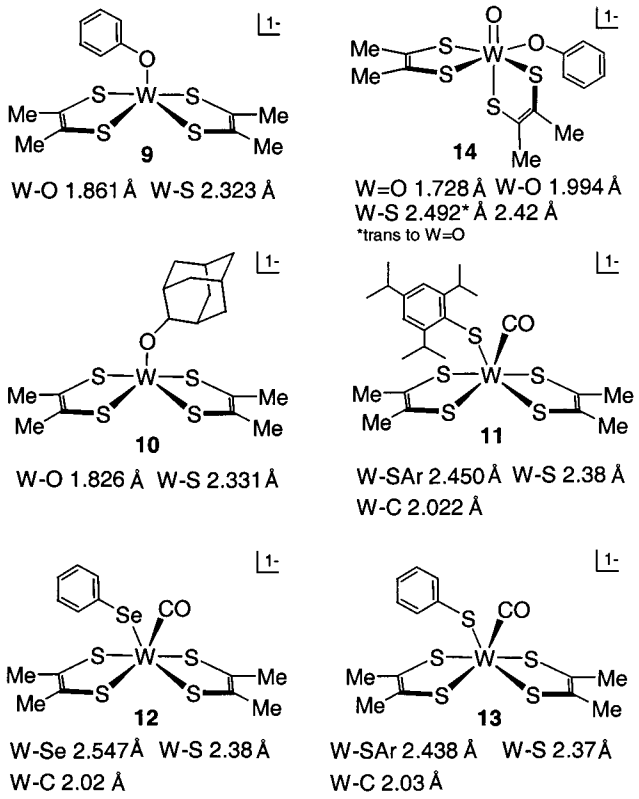

Figure 3. Schematic structures and selected mean bond lengths of bis(dithiolene)tungsten(IV,VI) complexes **9**−**14** as determined by X-ray crystallography.

Chart 1. Designations of Complexes[a]

$[Mo^{IV}O(S_2C_2Me_2)_2]^{2-}$	**1**[20]
$[Mo^{IV}(OSiBu^tPh_2)(S_2C_2Me_2)_2]^-$	**2**
$[Mo^{IV}(2\text{-}AdO)(S_2C_2Me_2)_2]^-$	**3**[25]
$[Mo^{IV}(OC_6H_2Pr^i_3)(S_2C_2Ph_2)_2]^-$	**4**[20]
$[Mo^{IV}(2\text{-}AdS)(S_2C_2Me_2)_2]^-$	**5**[25]
$[Mo^{IV}(SC_6H_2Pr^i_3)(S_2C_2Me_2)_2]^-$	**6**[20]
$[Mo^{IV}(2\text{-}AdSe)(S_2C_2Me_2)_2]^-$	**7**[25]
$[Mo^{IV}(CO)(SeC_6H_2Pr^i_3)(S_2C_2Me_2)_2]^-$	**8**[20]
$[W^{IV}(OPh)(S_2C_2Me_2)_2]^-$	**9**[22]
$[W^{IV}(2\text{-}AdO)(S_2C_2Me_2)_2]^-$	**10**[26]
$[W^{IV}(CO)(SC_6H_2Pr^i_3)(S_2C_2Me_2)_2]^-$	**11**[22]
$[W^{IV}(CO)(SePh)(S_2C_2Me_2)_2]^-$	**12**[22]
$[W^{IV}(CO)(SPh)(S_2C_2Me_2)_2]^-$	**13**[22]
$[W^{VI}O(OPh)(S_2C_2Me_2)_2]^-$	**14**[23]

[a] 2-Ad = 2-adamantyl.

Calcd for $C_{34}H_{47}MoNOS_4Si$: C, 55.33; H, 6.42; N, 1.90; S, 17.38; Si, 3.81. Found: C, 55.28; H, 6.35; N, 1.96; S, 17.40; Si, 3.88.

XAS Sample Preparation. The solid samples were ground into a fine powder in an inert atmosphere (dinitrogen) glovebox and diluted with boron nitride to maintain $\Delta\mu x \leq 1$ and prevent self-absorption. The mixture was pressed into a pellet and sealed between 63.5 μm Mylar tape windows in a 1 mm aluminum spacer. The samples were frozen in liquid nitrogen immediately upon removal from the glovebox and maintained at this or a lower temperature throughout storage and data collection.

XAS Data Collection. XAS data for all samples were measured at the Stanford Synchrotron Radiation Laboratory (SSRL) on unfocused beamline 7-3 under ring conditions of 3.0 GeV and 70−100 mA. A Si(220) double-crystal monochromator was utilized for energy selection at the respective edges (Se and Mo K-edges, W $L_{2,3}$-edges). The monochromator was detuned 50% at 13 776 eV (Se K-edge), 21 549 eV (Mo K-edge), 11 868 eV (W L_2-edge), and 11 326 eV (W L_3-edge) to minimize contamination from higher harmonics. An Oxford Instruments CF1208 continuous-flow liquid helium cryostat was used to maintain a constant sample temperature of 10 K. Data were collected in transmission mode with argon (Mo K-edge) or dinitrogen (Se K-edge and W L-edges) as the absorbing gas. The XAS data were measured to $k = 20$ Å^{-1} (Mo K-edge), $k = 9$ Å^{-1} (W L_2-edge), and $k = 17$ Å^{-1} (Se K-edge and W L_3-edges). Internal calibration was performed by simultaneous measurement of absorption edges of the corresponding elemental foil (powder) placed between a second and third ionization chamber. The first inflection point of the selenium powder spectrum was assigned to 12 658.0 eV, and that of the molybdenum spectrum, foil to 20003.9 eV. The first inflection point of the tungsten foil spectrum was assigned to 11 540.0 eV for the W L_2-edge and 10 202.0 eV for the W L_3-edge. The data represent averages of three to five scans for each sample.

XAS Data Analysis. The data analysis was performed using the ab initio GNXAS method. The theoretical basis for the GNXAS approach and its fitting methodologies have been described in detail elsewhere.[27−29]

(25) Lim, B. S.; Holm, R. H. *J. Am. Chem. Soc.*, submitted for publication.
(26) Sung, K.-M.; Holm, R. H. *J. Am. Chem. Soc.*, submitted for publication.

The program code generates theoretical EXAFS signals on the basis of an initial structural model. For the analysis reported here, the crystallographic coordinates for the corresponding complexes[20,22,23,25,26] were used to generate an initial structural model up to a distance cutoff of 5.0 Å. Phase shifts were calculated using the standard muffin-tin approximation to calculate the individual two- and three-body EXAFS signals. A model EXAFS spectrum was constructed by combining the individual component signals and an appropriate background. This model was then fit to the averaged raw absorption data by a least-squares minimization program that uses the MINUIT subroutine of the CERN library. Background subtraction was performed by applying a flexible three-segment spline which was refined in the GNXAS fits. The quality of the fit was calculated by the least-squares residual R and monitored by visual inspection of the fits to the data and their Fourier transforms (FTs) and of the residual EXAFS signal and its FT. The structural parameters varied during the refinements were the bond distance (R) and the bond variance $(\sigma_R^2)^2$ in the case of a two-body signal and the two shorter bond distances R_1 and R_2, the intervening angle (θ), and the six covariance matrix elements for a three-body signal. The nonstructural parameters E_o and S_o^2 were varied, whereas Γ_C (core hole lifetime) and E_r (experimental resolution) were kept fixed to physically reasonable values throughout the analysis. The coordination numbers were set to the values determined by X-ray crystallography. All parameters were varied within a preset range, and all results were checked to ensure that values obtained did not reach the high or low points of these fitting ranges. The molybdenum data were fit over the k range 3.5−19.5 Å^{-1}, and the selenium and tungsten data over the k range 3.5−17 Å^{-1}.

Results

Edges. (a) Molybdenum K-Edges. The edge data for molybdenum complexes **3**, **5**, and **7** containing the ligand 2-AdQ (Q = O, S, Se) are shown in Figure 4 together with their second derivatives. While the formal oxidation state remains the same in all three complexes, there is a shift in the edge position consistent with the relative electronegativity of the ligand. Complex **3** (AdO) is shifted ∼1.4 eV higher in energy compared to **7** (AdSe), with **5** (AdS) in an intermediate position, ∼0.4 eV lower than **7**. The numbers, intensities, and positions of the transitions superimposed on the rising edge show variations that can be more clearly seen in the second-derivative spectra. The edge structure consists of three (**3**) or four (**5**, **7**) transitions. All three complexes have one transition between 20 002 and 20 004 eV and one between 20 014 and 20 015 eV. Both of these transitions show a shift consistent with the electronegativity of the AdQ ligand, with the transitions of **3** shifted to highest energy. The largest differences occur in the region between 20 023 and 20 031 eV, where **3** exhibits a single transition at ∼20 030 eV and **5** and **7** show two lower intensity transitions at 20 023 and 20 031 eV (transitions are less resolved in **7**). The differences must result from variation of the AdQ ligand (Q = O, S, Se), as these square pyramidal complexes are otherwise structurally analogous. These molecules thus allow us to investigate the effect of different terminal ligand types on XAS edge features and represent an important set of complexes for our studies aimed at establishing fingerprints of the DMSOR family of enzymes. The active sites of these enzymes have a single protein ligand bound to the molybdenum atom, the identity of which distinguishes the sites (Figure 1). The variation of the terminal ligand in **3**, **5**, and **7** correlates with changes in the protein ligand.

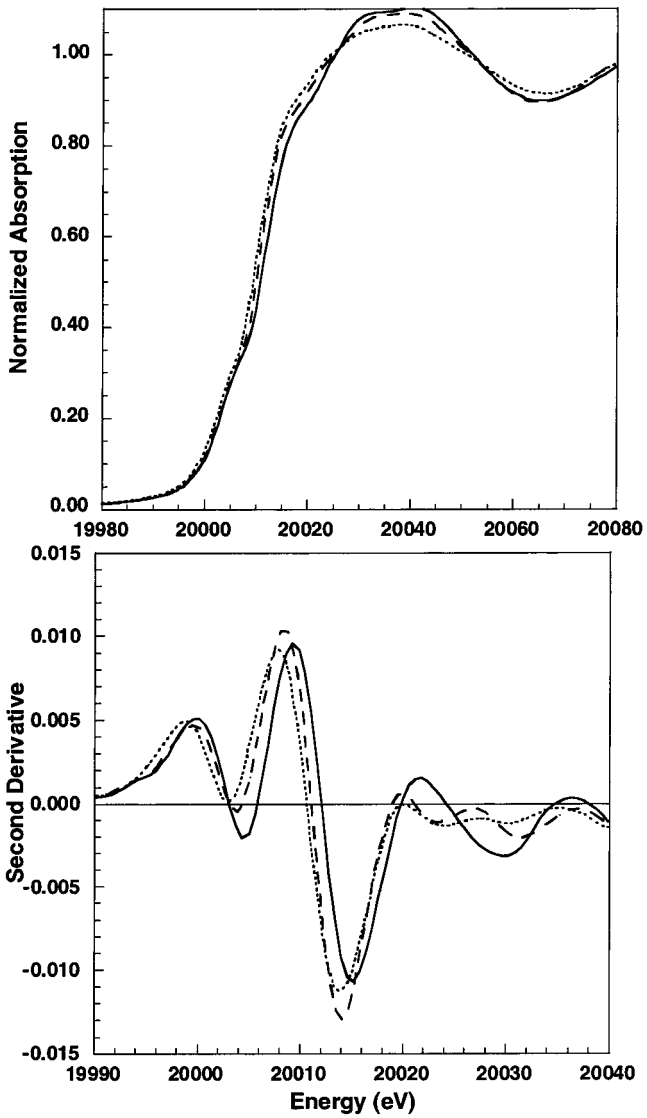

Figure 4. Normalized Mo-K edge spectra of $[Mo^{IV}(2\text{-AdO})(S_2C_2Me_2)_2]^-$ (**3**, —), $[Mo^{IV}(2\text{-AdS})(S_2C_2Me_2)_2]^-$ (**5**, - - -), and $[Mo^{IV}(2\text{-AdSe})(S_2C_2Me_2)_2]^-$ (**7**, ···) with the corresponding second-derivative spectra shown below. See text for a detailed description of the edge structure.

Complexes **1**−**4** contain one oxygen ligand, multiply bound in oxo complex **1** and singly bound in **2**−**4**. As previously shown,[7,24,30,31] the presence of a Mo═O bond dramatically affects the intensity of the transition at ∼20 008 eV and is often used to identify the presence and number of oxo groups in a given molecule (see Supporting Information, Figure S1). For complexes **2**−**4**, there are no significant differences in the positions, numbers, or intensities of the transitions superimposed on the rising edge. (Slight variations in intensity are attributed to different ligand structures). The same is true for complexes **5** and **6**, both containing five sulfur ligands, as their edges are superimposable (Figure S2 (Supporting Information)). This behavior is expected, as the edge is more sensitive to changes in the ligating atom type than to other ligand structural differences further removed from the photoabsorber.

Differences between selenolate complexes **7** and **8** are attributed to a change in coordination number from 5 to 6. The

(27) Filipponi, A.; Di Cicco, A.; Tyson, T. A.; Natoli, C. R. *Solid State Commun.* **1991**, *78*, 2265.
(28) Filipponi, A.; Di Cicco, A.; Natoli, C. R. *Phys. Rev. B* **1995**, *52*, 15122.
(29) Westre, T. E.; Di Cicco, A.; Filipponi, A.; Natoli, C. R.; Hedman, B.; Solomon, E. I.; Hodgson, K. O. *J. Am. Chem. Soc.* **1995**, *117*, 1566.
(30) Kutzler, F. W.; Natoli, C. R.; Misemer, D. K.; Doniach, S.; Hodgson, K. O. *J. Chem. Phys.* **1980**, *73*, 3274.
(31) Kutzler, F. W.; Scott, R. A.; Berg, J. M.; Hodgson, K. O.; Doniach, S.; Cramer, S. P.; Chang, C. H. *J. Am. Chem. Soc.* **1981**, *103*, 6083.

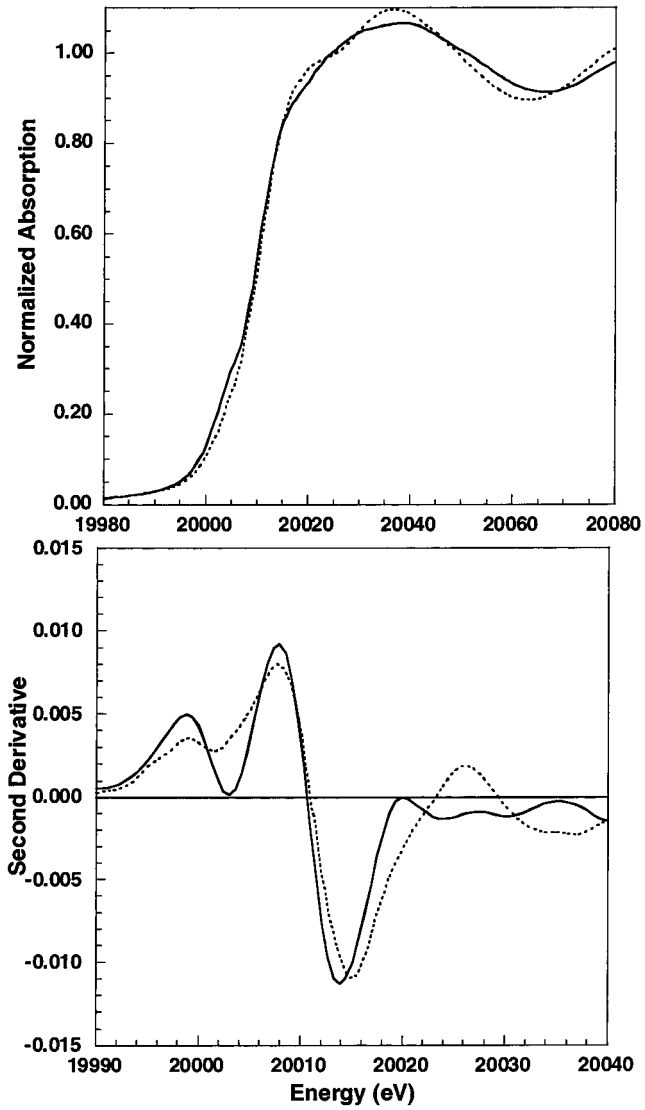

Figure 5. Normalized Mo-K edge spectra of $[Mo^{IV}(2\text{-AdSe})(S_2C_2Me_2)_2]^-$ (**7**, —) and $[Mo^{IV}(CO)(SeC_6H_2Pr^i_3)(S_2C_2Me_2)_2]^-$ (**8**, ···) with the corresponding second-derivative spectra shown below. Significant differences can be seen resulting from the presence of a CO ligand in **8**, as discussed in the text.

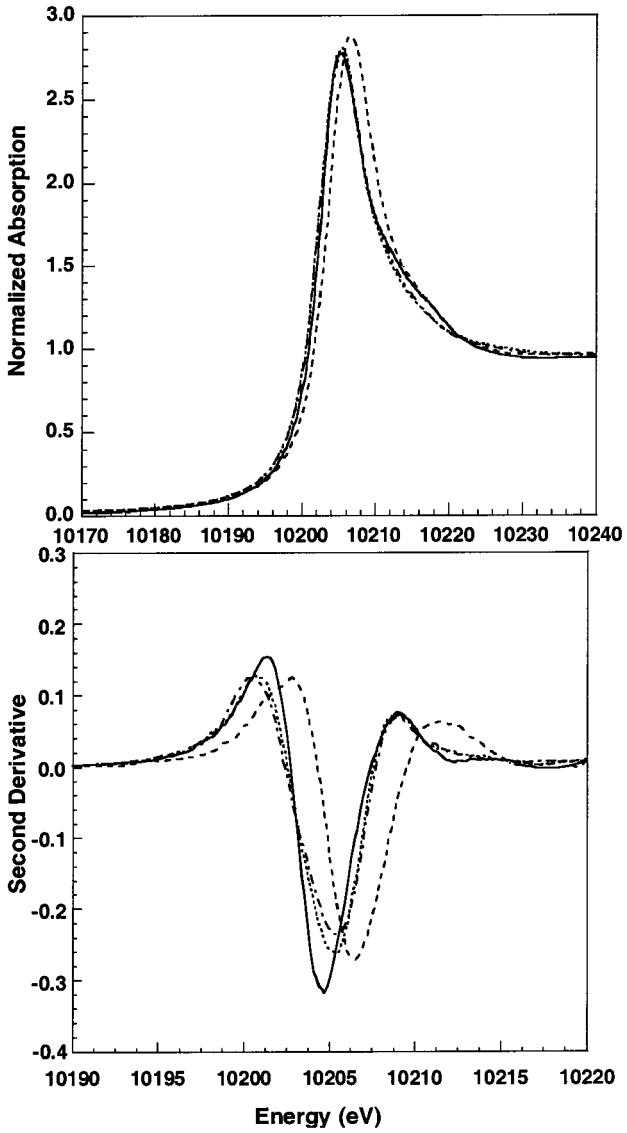

Figure 6. Normalized W-L_3 edge spectra of $[W^{IV}(2\text{-AdO})(S_2C_2Me_2)_2]^-$ (**10**, —), $[W^{IV}(CO)(SC_6H_2Pr^i_3)(S_2C_2Me_2)_2]^-$ (**11**, —·—), $[W^{IV}(CO)(SePh)(S_2C_2Me_2)_2]^-$ (**12**, - - -), and $[W^{VI}O(OPh)(S_2C_2Me_2)_2]^-$ (**14**, ···). These spectra show a relatively featureless rising edge with a very intense peak or "white-line" which is correlated to the unfilled d valence states. Data for **9** and **13** are omitted for clarity, as they are identical to those for **10** and **11**, respectively.

presence of a CO ligand in **8** does not affect the position of the edge but does lead to significant changes in the shapes, numbers, and intensities of the transitions superimposed along it, as seen in Figure 5. As clearly displayed by the second derivative, the first transition of **8** is shifted to lower energy by ~2 eV and has ~75% less intensity. The second transition of **8** has about the same intensity as that of **7**, but it is shifted to higher energy by ~2 eV and the peak has become more broad, as a shoulder has appeared. The two transitions between 20 023 and 20 031 eV for **7** are absent in the case of **8**, which exhibits a third transition centered at 20 035 eV.

In our previous work with bdt complexes,[24] we observed that the type of dithiolene ligand should have little effect on the molybdenum edge and its features. Complex **2** was prepared in order to examine that point. The nearly superimposable edges of **2** and $[Mo(OSiBu^tPh_2)(bdt)_2]^-$ (shown previously[24]) are a satisfactory demonstration that dithiolene ligands $S_2C_2Me_2$ and bdt are indistinguishable from an XAS-edge standpoint (Figure S3 (Supporting Information)).

(b) Tungsten L-Edges. The tungsten L_3-edge spectra of complexes **9**−**14** show a relatively featureless rising edge with a very intense peak or "white-line" that is correlated to unfilled 5d valence states. These peaks are due to a strong dipole-allowed, bound state transition from the $2p_{3/2}$ initial state to vacant 5d orbitals. Spectra of four complexes are presented in Figure 6. The overall shapes and intensities of these peaks are similar for all of the complexes, with a slightly broader peak (~0.3 eV fwhm) for the six-coordinate complexes **11**−**14**. There are very minor shifts in the edge positions for complexes **10**−**13**, which appear related to ligand electronegativities. There is a large shift in the position of the edge for **14** relative to the others, consistent with a change in oxidation state from W^{IV} to W^{VI}. The trends seen in the L_3-edges are also observed in the L_2-edges (data not shown) which result from a strong dipole-allowed bound state transition from the $2p_{1/2}$ initial state to vacant 5d orbitals.[32]

(c) Selenium K-Edges. The selenium K-edge spectra of

(32) Lye, R. C.; Phillips, J. C.; Kaplan, D.; Doniach, S.; Hodgson, K. O. *Proc. Natl. Acad. Sci. U.S.A.* **1980**, *77*, 5884.

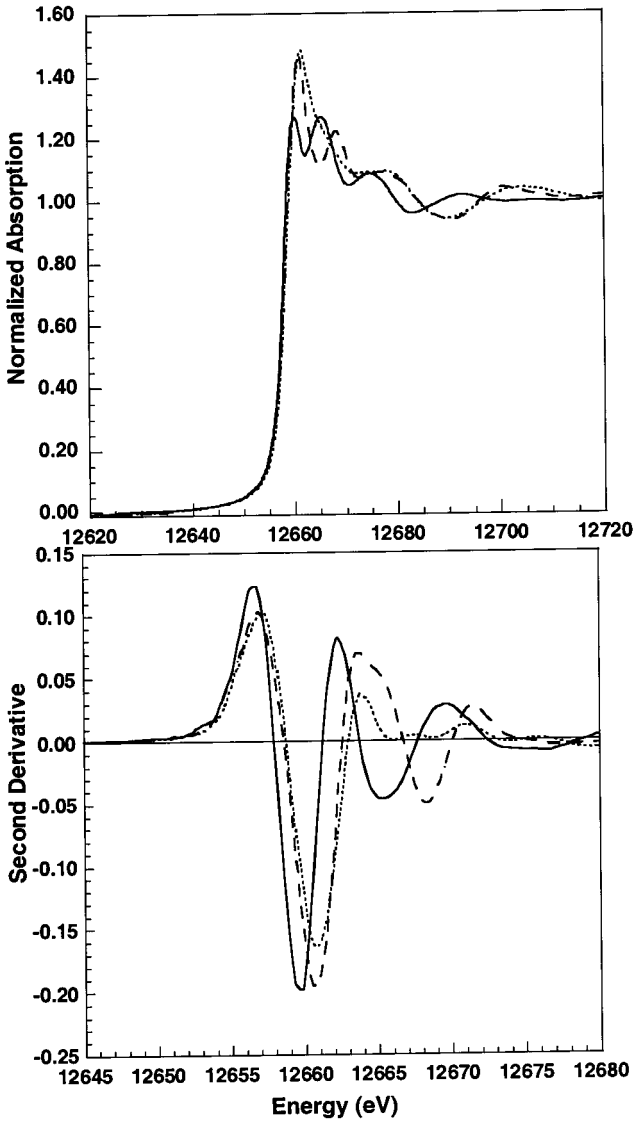

Figure 7. Normalized Se-K edge spectra of $[Mo^{IV}(2\text{-AdSe})(S_2C_2Me_2)_2]^-$ (**7**, —), $[Mo^{IV}(CO)(SeC_6H_2Pr^i_3)(S_2C_2Me_2)_2]^-$ (**8**, - - -), and $[W^{IV}(CO)(SePh)(S_2C_2Me_2)_2]^-$ (**12**, ···), with the corresponding second-derivative spectra shown below. See text for detailed description of the edge structure.

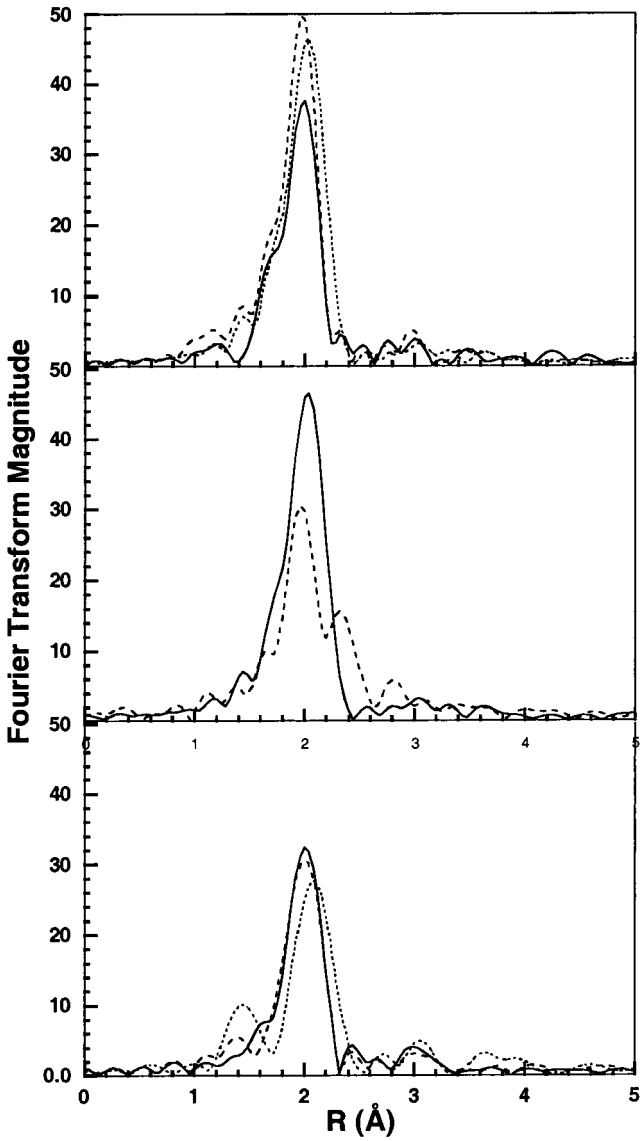

Figure 8. Comparison of the non-phase-shift-corrected Mo K-edge Fourier transforms of $[Mo^{IV}(2\text{-AdO})(S_2C_2Me_2)_2]^-$ (**3**, —), $[Mo^{IV}(2\text{-AdS})(S_2C_2Me_2)_2]^-$ (**5**, - - -), and $[Mo^{IV}(2\text{-AdSe})(S_2C_2Me_2)_2]^-$ (**7**, ···) (top), $[Mo^{IV}(2\text{-AdSe})(S_2C_2Me_2)_2]^-$ (**7**, —) and $[Mo^{IV}(CO)(SeC_6H_2Pr^i_3)(S_2C_2Me_2)_2]^-$ (**8**, - - -) (middle), and W L_3-edge Fourier transforms of $[W^{IV}(OPh)(S_2C_2Me_2)_2]^-$ (**9**, —), $[W^{IV}(2\text{-AdO})(S_2C_2Me_2)_2]^-$ (**10**, - - -), and $[W^{VI}O(OPh)(S_2C_2Me_2)_2]^-$ (**14**, ···) (bottom).

complexes **7**, **8**, and **12** are shown in Figure 7 together with their second derivatives. Complexes **8** and **12**, with aromatic selenolate ligands, are structural molybdenum and tungsten analogues. There is no shift in the energy position for the main transition around 12 661 eV, as measured by the first inflection point of the two spectra. However, on the high-energy side, the data for **8** are characterized by one well-resolved feature, while those for **12** show two overlapping features of low intensity. This difference is most likely due to the type of metal backscatterer. The edge for **7** shows a main transition that is shifted to lower energy by ~1 eV, with the most prominent differences relative to **8** being the sharp reduction in intensity for this transition and the proximity of a second higher energy transition at ~12 665 eV of similar intensity. There are two differences between **7** and **8**: the presence of a carbonyl ligand (**8**), which will influence the electronic structure of the selenium atom, and aliphatic vs aromatic selenolates. In the absence of a more extensive database, we are unable to relate edge differences to these factors.

Fourier Transforms. (a) Molybdenum K-Edge. The bond distance trends seen in the FTs agree with those determined by X-ray crystallography. While distances cannot be directly determined from FTs, owing to uncertainty in phase shift corrections and interference effects, they clearly visualize the various frequency components that contribute to the overall EXAFS wave. The Fourier transforms of complexes **3**, **5** and **7**, all containing the 2-AdQ ligand (Q = O, S, Se), have one main peak that shows variation in both intensity and position, as seen in Figure 8 (top panel). The peak intensity is highest for **5**, which contains five equidistant Mo−S bonds. The positions of the peak are similar for **3** and **5**; however, the intensity is ~30% lower for **3**. This behavior results from both a smaller number of sulfur ligands and the presence of a lighter oxygen ligand in **3**, whose EXAFS contribution destructively interferes with the Mo−S wave. For **7**, this single peak has approximately the same intensity but is slightly broader and has shifted to a higher *R* value by ~0.15 Å, an effect attributed to the presence of a longer Mo−Se interaction in addition to

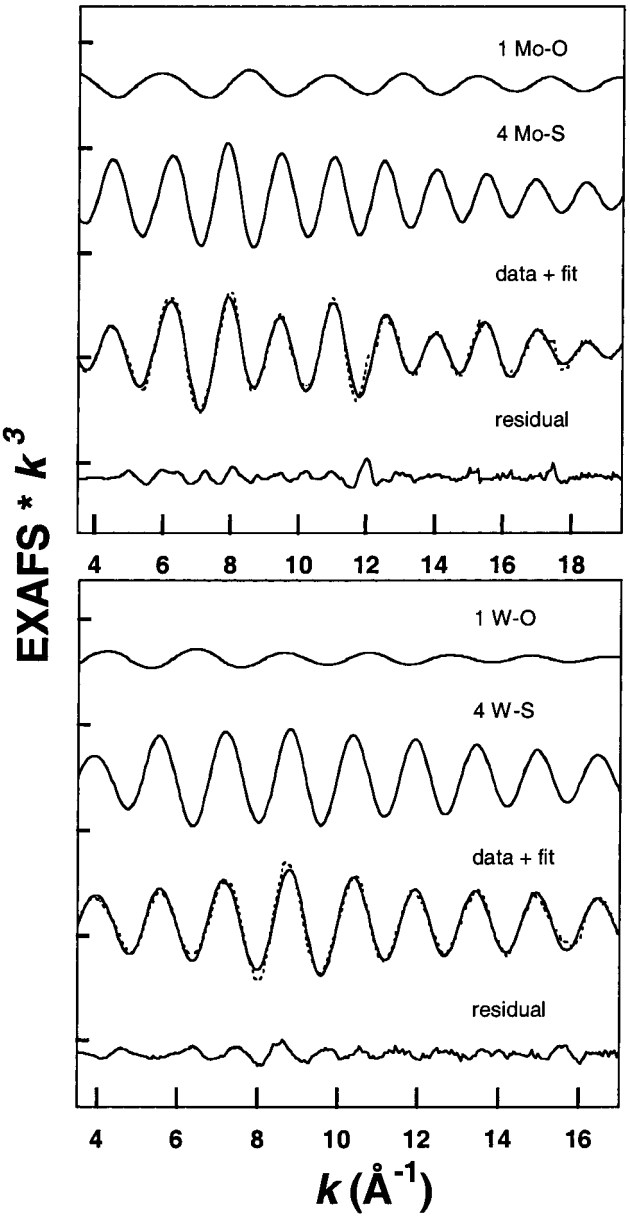

Figure 9. Individual EXAFS contributions and total EXAFS signals (—) compared with the experimental Mo K- and W L_3-edge EXAFS data (- - -) for $[Mo^{IV}O(S_2C_2Me_2)_2]^-$ (**1**, top) and $[W^{IV}(2\text{-AdO})(S_2C_2Me_2)_2]^-$ (**10**, bottom). (The ordinate scale is 15 units between tick marks.)

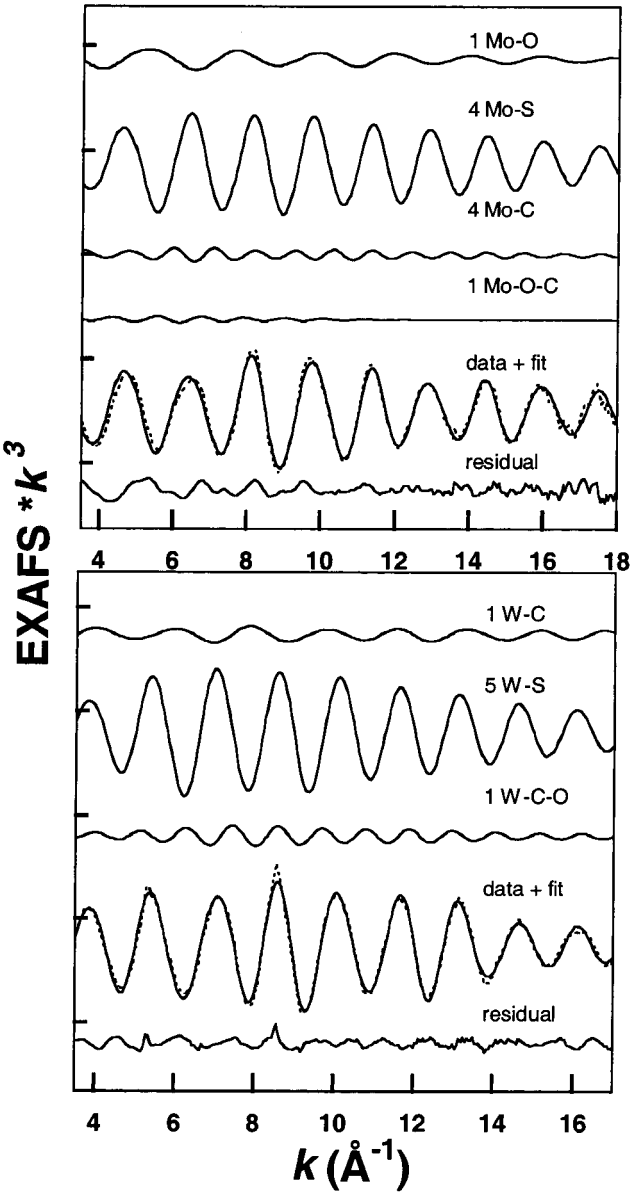

Figure 10. Individual EXAFS contributions and total EXAFS signals (—) compared with the experimental Mo K- and W L_3-edge EXAFS data (- - -) for $[Mo^{IV}(OC_6H_2Pr^i_3)(S_2C_2Me_2)_2]^-$ (**4**, top) and $[W^{IV}(CO)(SPh)(S_2C_2Me_2)_2]^-$ (**13**, bottom). (The ordinate scale is 15 units between tick marks.)

the Mo−S interaction. The distance separation between these two interactions broadens the peak but is not large enough to result in two resolvable peaks in the FT.

A number of similarities exist between the other molybdenum complexes and those containing the 2-AdQ ligand. When differences are seen, they are mainly a result of the unique fifth ligand or the presence of a sixth ligand. Several differences are seen in the FTs of oxygen-containing complexes **1**, **2**, and **4** when compared to that of **3** (Figure S4 (Supporting Information)). The FT of **1** shows an additional peak at ∼1.4 Å, resulting from the presence of a short Mo═O bond. The main peak is shifted to a higher *R* value and has a slightly decreased intensity. This behavior is attributed to the longer Mo−S bond length and the noncontribution of the short Mo═O interaction to this peak, in contrast to the effect of longer Mo−O interactions in other complexes. For **2** and **4**, the intensities and positions of the main peaks are similar to those of **3**; however, both exhibit an additional low-intensity peak visible above the noise level at about 3.2 Å (**2**) and 2.9 Å (**4**). The EXAFS results discussed below show that these features result from nearly linear multiple-scattering interactions involving the Mo−O−Si and Mo−O−C pathways in **2** and **4**, respectively.

There are no significant differences in the peak intensities or positions for **5** and **6**, both of which contain five sulfur ligands at similar distances. A number of differences exist between the two selenolate complexes **7** and **8** (Figure 8, middle panel). Complex **8** is six-coordinate and contains a carbonyl ligand in a linear M−CO arrangement, which, in addition to contributing to the first peak in the FT, gives rise to a low-intensity multiple-scattering feature at ∼2.8 Å. In addition, the greater separation between the Mo−S and Mo−Se bond lengths (0.12 Å (**7**) and 0.22 Å (**8**), Figure 2) results in a splitting of the single peak of **7** into two resolvable, less intense peaks for **8**.

(b) Tungsten L_3-Edge. The FTs of the six-coordinate carbonyl complexes **11**−**13** (Figure S5 (Supporting Informa-

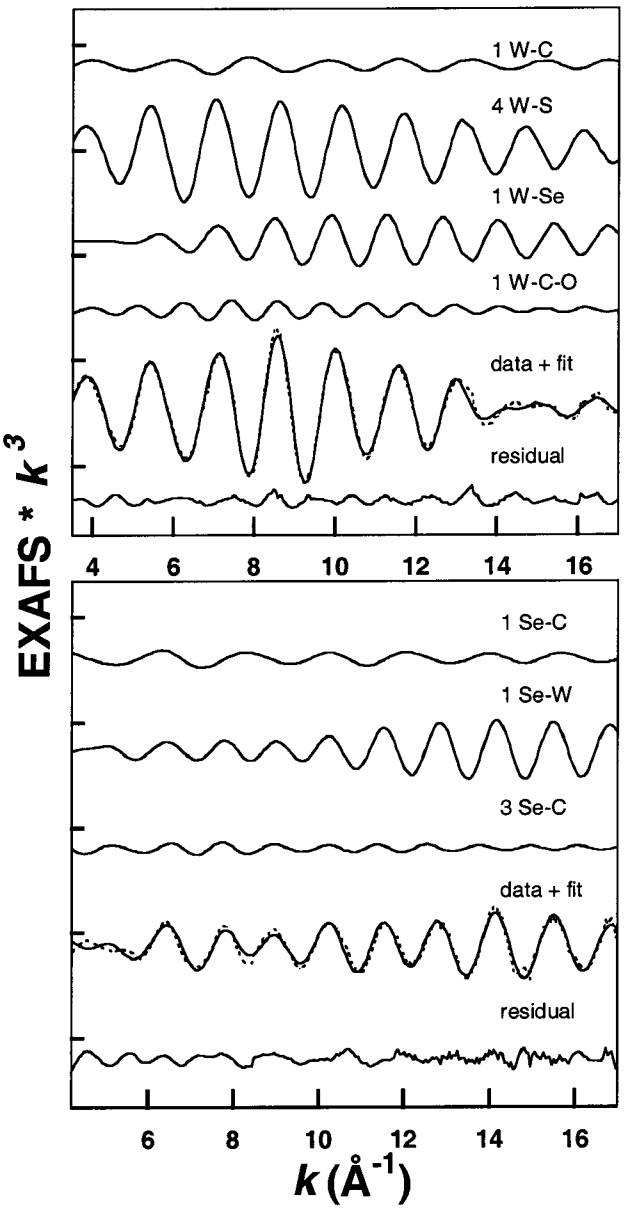

Figure 11. Individual EXAFS contributions and total EXAFS signals (—) compared with the experimental EXAFS data (- - -) for $[W^{IV}(CO)(SePh)(S_2C_2Me_2)_2]^-$ (**12**): (top) W L_3-edge EXAFS; (bottom) Se K-edge EXAFS. (The ordinate scale is 15 units between tick marks.)

tion)) all contain two peaks, an intense feature centered at ~2.0 Å (resulting from W−C, W−S, and W−Se ligations) and an 80% less intense feature at ~2.9 Å (attributed to multiple scattering from the CO ligand). The intensity ratio of the two peaks is the same for the three complexes, the only notable difference being the slightly broadened main peak for **12**, resulting from the presence of a longer W−Se interaction in addition to the W−S interaction.

The FTs of the structurally analogous oxygen-containing complexes **9** and **10** are superimposable, both having a single peak at ~1.9 Å composed of both W−O and W−S waves. Differences between **9**/**10** and distorted octahedral **14** are seen in the bottom panel of Figure 8. The FT of **14** contains two peaks: a low-*R* peak at ~1.4 Å attributed to the short W═O bond not present in the other compounds and a second peak that is shifted by 0.2 Å and is slightly less intense relative to the main peaks for **9** and **10**. The shift is consistent with the longer W−S distance determined for **14**. The decreased intensity results from slightly different interference patterns between the three waves contributing to the Fourier transform. These complexes do not exhibit any other peaks resolvable above the noise level, and multiple-scattering interactions were not found to be important in the EXAFS analysis.

The Mo K- and W L_3-edge FTs for structurally analogous complexes such as the oxygen-containing set (**2**−**4**, **9**, **10**) are very similar in terms of peak positions and intensities. This is expected, as the crystallographic bond distances (Figures 1 and 2) are within ±0.03 Å of one another. Differences are seen between selenium-containing **8** and **12**, as the main peak of **8** has split into two distinct peaks. This is due to a combination of the greater separation between the Mo−S and Mo−Se distances (0.22 Å in **8** as compared to 0.17 Å in **12**) and the larger *k* range of the data for **8**, both of which result in better resolution.

(c) Selenium K-Edge. The FTs of **8** and **12** are very similar (Figure S6 (Supporting Information)). Both contain a low-*R* peak centered at ~1.7 Å resulting from a Se−C bond and a second, much more intense peak arising from Se−Mo/W ligation. The variation of ~0.15 Å in the positions of the second peak can be attributed to differences in the phase shifts between Se−Mo (**8**) and Se−W (**12**), as the distances determined by X-ray crystallography and the EXAFS analysis (vide infra) are quite similar for both complexes. For **7**, the intensity of the main peak has increased by ~25% and the peak has shifted to lower *R*, consistent with the presence of a shorter Se−Mo distance. The resulting interference pattern between waves leads to less destructive interference than seen for **8** and **12**.

The FTs of the set of 14 molybdenum and tungsten complexes serve as diagnostic indicators of the different coordination spheres. While they are useful to visualize various frequency components, a detailed EXAFS fitting analysis is required to extract highly accurate metrical information.

EXAFS Analysis. GNXAS fits were performed by utilizing phase and amplitude functions calculated from crystallographic coordinates. EXAFS signals and fits for complexes **1**, **4**, **10**, **12**, and **13** are presented in Figures 9−11. Fits of other complexes not shown are comparable to these (Figures S7 and S8 (Supporting Information)). The quality of the data for all 14 complexes is very high, as judged by the low noise level at the high-*k* ranges of the data (an exception is noted in the case of **8**, for which a high noise level prevented the use of $k \geq 18$ $Å^{-1}$ data). GNXAS fit results are summarized in Tables 1−3 for molybdenum, tungsten, and selenium species, respectively.[33] Our results show a variance of ≤0.02 Å among bond lengths determined by EXAFS and crystallography, including average values for molecules in which two distinct M−S distances were determined crystallographically (**6**, **11**, **13**, **14**).

For clarity, fits are broken down into those containing only single-scattering interactions (**1**, **3**, **5**−**7**, **9**, **10**, **14**) and those that required both single and multiple scattering (**2**, **4**, **8**, **11**-**13**). Oxygen-ligated complexes **1**, **3**, **9**, and **10** could be accurately fit with inclusion of two waves, an M−O interaction with a coordination number of 1 and an M−S interaction with a coordination number of 4. Individual EXAFS contributions and the total EXAFS signal compared with the experimental EXAFS data for **1** and **10** can be seen in Figure 9. The Mo−O distance in complex **1** is much shorter than that of the other

(33) Attempts were made to fit distant scattering from carbon atoms of terminal ligands, as a small high-frequency beat pattern can be seen in the EXAFS fit residual (Figures 8−10). Inclusion of longer single- and multiple-scattering interactions did not lead to statistically significant improvements in the fits.

Table 1. GNXAS Fit Results of Mo K-Edge EXAFS Analysis[a]

	Mo−Q[b]			Mo−S			additional contributions					
	N	*R* (Å)	σ^2 (Å^2)	*N*	*R* (Å)	σ^2 (Å^2)		*N*	*R* (Å)	σ^2 (Å^2)	angle (deg)	*R*
$[Mo^{IV}O(S_2C_2Me_2)_2]^{2-}$ (**1**)	1	1.71	0.001	4	2.40	0.002						0.174×10^{-7}
$[Mo^{IV}(OSiBu^tPh_2)(S_2C_2Me_2)_2]^-$ (**2**)	1	1.86	0.001	4	2.35	0.002	Mo−O−Si	1	3.48	0.002	175	0.860×10^{-8}
$[Mo^{IV}(2\text{-AdO})(S_2C_2Me_2)_2]^-$ (**3**)	1	1.85	0.003	4	2.35	0.002						0.115×10^{-6}
$[Mo^{IV}(OC_6H_2Pr^i_3)(S_2C_2Ph_2)_2]^-$ (**4**)	1	1.84	0.002	4	2.33	0.002	Mo−C	4	3.33	0.003		0.478×10^{-7}
							Mo−O−C	1	3.29	0.005	177	
$[Mo^{IV}(2\text{-AdS})(S_2C_2Me_2)_2]^-$ (**5**)				5	2.34	0.002						0.116×10^{-6}
$[Mo^{IV}(SC_6H_2Pr^i_3)(S_2C_2Me_2)_2]^-$ (**6**)				5	2.34	0.003						0.367×10^{-7}
$[Mo^{IV}(2\text{-AdSe})(S_2C_2Me_2)_2]^-$ (**7**)	1	2.46	0.002	4	2.34	0.002						0.386×10^{-7}
$[Mo^{IV}(CO)(SeC_6H_2Pr^i_3)(S_2C_2Me_2)_2]^-$ (**8**)	1	2.59	0.002	4	2.37	0.002	Mo−C	1	2.03	0.003		0.665×10^{-7}
							Mo−C−O	1	3.18	0.006	178	

[a] In the fits, the following parameters were refined: E_0, S_0^2, *R*, and the corresponding σ^2 values as well as the six covariance matrix elements. [b] Q refers to either Mo−O or Mo−Se ligation in the corresponding complexes. The E_0 values varied less than 1 eV and the S_0^2 values less than 0.05 over all fits reported. The coordination numbers (*N*) were set to the values determined by X-ray crystallography. The Γ_0 and experimental resolution parameters were fixed to physically reasonable values throughout the analysis. See text for definitions of the above-mentioned parameters.

Table 2. GNXAS Fit Results of W L_3-Edge EXAFS Analysis[a]

	W−Q[b]			W−S			additional contributions					
	N	*R* (Å)	σ^2 (Å^2)	*N*	*R* (Å)	σ^2 (Å^2)		*N*	*R* (Å)	σ^2 (Å^2)	angle (deg)	*R*
$[W^{IV}(OPh)(S_2C_2Me_2)_2]^-$ (**9**)	1	1.86	0.001	4	2.33	0.002						0.979×10^{-6}
$[W^{IV}(2\text{-AdO})(S_2C_2Me_2)_2]^-$ (**10**)	1	1.82	0.003	4	2.34	0.002						0.607×10^{-7}
$[W^{IV}(CO)(SC_6H_2Pr^i_3)(S_2C_2Me_2)_2]^-$ **11**				5	2.39	0.004	W−C	1	2.00	0.001		0.368×10^{-6}
							W−O−C	1	3.19	0.004	180	
$[W^{IV}(CO)(SePh)(S_2C_2Me_2)_2]^-$ (**12**)	1	2.55	0.002	4	2.38	0.004	W−C	1	2.02	0.001		0.143×10^{-6}
							W−O−C	1	3.18	0.003	180	
$[W^{IV}(CO)(SPh)(S_2C_2Me_2)_2]^-$ (**13**)				5	2.39	0.003	W−C	1	2.03	0.001		0.310×10^{-7}
							W−O−C	1	3.18	0.003	180	
$[W^{VI}O(OPh)(S_2C_2Me_2)_2]^-$ (**14**)	1	2.00	0.004	4	2.43	0.003	W═O	1	1.73	0.001		0.631×10^{-7}

[a] In the fits, the following parameters were refined: E_0, S_0^2, *R*, and the corresponding σ^2 values as well as the six covariance matrix elements. [b] Q refers to either W−O or W−Se ligation in the corresponding complexes. The E_0 values varied less than 1.2 eV and the S_0^2 values less than 0.03 over all fits reported. The coordination numbers (*N*) were set to the values determined by X-ray crystallography. The Γ_0 and experimental resolution parameters were fixed to physically reasonable values throughout the analysis. See text for definitions of the above-mentioned parameters.

Table 3. GNXAS Fit Results of Se K-Edge EXAFS Analysis[a]

	short Se−C			Se-M[b]			long Se−C			
	N	*R* (Å)	σ^2 (Å^2)	*N*	*R* (Å)	σ^2 (Å^2)	*N*	*R* (Å)	σ^2 (Å^2)	*R*
$[Mo^{IV}(2\text{-AdSe})(S_2C_2Me_2)_2]^-$ (**7**)	1	2.02	0.001	1	2.46	0.001	2	2.96	0.002	0.386×10^{-5}
$[Mo^{IV}(CO)(S_2C_2Me_2)_2(SeC_6H_2Pr^i_3)]^-$ (**8**)	1	1.94	0.001	1	2.57	0.001	3	2.96	0.002	0.121×10^{-6}
$[W^{IV}(CO)(S_2C_2Me_2)_2(SePh)]^-$ (**12**)	1	1.96	0.001	1	2.56	0.003	3	2.90	0.002	0.124×10^{-6}

[a] In the fits, the following parameters were refined: E_0, S_0^2, *R*, and the corresponding σ^2 values as well as the six covariance matrix elements. [b] M refers to either Se−Mo or Se−W ligation in the corresponding complexes. The E_0 values varied less than 1.3 eV and the S_0^2 values less than 0.03 over all fits reported. The coordination numbers (*N*) were set to the values determined by X-ray crystallography. The Γ_0 and experimental resolution parameters were fixed to physically reasonable values throughout the analysis. See text for definitions of the above-mentioned parameters.

oxygen-containing complexes (1.71 Å vs an average value of 1.84 Å). This is in agreement with both the Mo K-edge data and the FT, which shows a clearly resolved low-*R* peak, indicating the presence of an oxo group. The longer M−O distances in the other complexes are in agreement with the presence of a singly bound oxygen ligand. For complex **14** (Figure S7), waves at two distinct W−O distances are required, a short W═O distance at 1.73 Å and a longer W−O distance at 2.00 Å, in addition to the W−S interaction with a coordination number of 4. The average M−S distances are longer in oxo complexes **1** and **14** than in **3**, **9**, and **10** (2.42 Å vs. 2.34 Å).

Complexes **5** and **6** require inclusion of a single Mo−S interaction at 2.34 Å with a coordination number of 5. Selenolate complex **7** is well fit by Mo−Se and Mo−S waves with coordination numbers of 1 and 4 at 2.46 and 2.34 Å, respectively. None of these complexes require inclusion of any additional components, as indicated by the low fit residual and the absence of any other features in the FTs.

Six complexes require inclusion of multiple-scattering interactions in addition to single scattering. Fits for **4** and **13** are presented in Figure 10, and the fits for **12**, which include data from the W L_3-edge and the Se K-edge, are shown in Figure 11. Acceptable fits of the data for **8** and **11**−**13** all necessitate inclusion of the nearly linear M−C−O multiple-scattering pathway in addition to M−C, M−O/Se, and M−S single-scattering interactions (Tables 1 and 2). It has previously been shown that multiple-scattering interactions are very sensitive to angles between 150 and 180°.[29,34] When these interactions are included, the distant peaks in the FTs are well fit and the *R* values of the fits decrease significantly. In all cases, the M−C−O angle is found to be best fit at 178−180°.

In the case of **2** (Figure S8), a nearly linear Mo−O−Si interaction is needed to fit the peak in the FT at 3.2 Å. Fits for **4** (Figure 10) require inclusion of two additional waves, a Mo−C single-scattering interaction at 3.3 Å with a coordination number of 4 and a Mo−O−C multiple-scattering interaction; both result from ring carbon scattering of the terminal ligand. In this case, the Mo−O−C angle fit best at 177°, which is the crystallographic value. Inclusion of ring carbon scattering was not necessary for the other complexes, as the M−Q−C angles are considerably smaller (103−147°), preventing them from con-

(34) Zhang, H. H.; Filipponi, A.; Di Cicco, A.; Lee, S.; Scott, M. J.; Holm, R. H.; Hedman, B.; Hodgson, K. O. *Inorg. Chem.* **1996**, *35*, 4819.

tributing significantly to the EXAFS. In addition, the high-*R* region of the FTs gives no indication of such contribution. The bond distances and their corresponding bond variances, as well as the nonstructural parameters which were allowed to float during the fitting, remain almost constant in both the single- and multiple-scattering fits, implying in either case that the parameters are well fit. In all cases, the ×c2 value of the fit decreases significantly (between 20 and 30%) upon inclusion of the multiple-scattering pathways.

The selenium EXAFS data for complexes **7**, **8**, and **12** were also analyzed. The M−Se distances determined from the corresponding molybdenum and tungsten EXAFS analyses are within ±0.02 Å of the values obtained from the selenium analysis. Our ability to measure more than one XAS edge of a given molecule provides a means to check the internal consistency of the determined bond distances. Fits to the selenium EXAFS data only required inclusion of single-scattering interactions. For all three molecules, short Se−C and Se−M interactions and a longer Se−C interaction are needed to achieve acceptable fits to the data.

Summary and Conclusions

Molybdenum and selenium K-edge and tungsten $L_{2,3}$-edge spectra have been obtained and the EXAFS data analyzed using the GNXAS protocol for a set of 14 bis(dithiolene)molybdenum and -tungsten complexes (Figures 2 and 3). The set includes six five-coordinate and one six-coordinate Mo^{IV}, two five-coordinate and three six-coordinate W^{IV}, and one six-coordinate W^{VI} complexes. The numbers, intensities, and positions of the transitions superimposed on the rising edges exhibit variations related to the type and number of ligands bound to the metals, a behavior best appreciated from second-derivative spectra (Figures 4−6). The FTs of the set of complexes serve as diagnostic indicators of the various coordination spheres. They can be used to evaluate variations in coordination number, ligand type (oxygen, sulfur, or selenium), and distance separations in the case of well-resolved peaks. Accurate structures of all but **2** are available,[20,22,23,25,26] permitting an assessment of the accuracy of structural parameters derived from XAS. Further, chelation is symmetrical and chelate ring bond lengths from crystallography point to the ene-1,2-dithiolate ligand oxidation level, leading to the indicated metal oxidation state assignments. The following are the principal conclusions from this investigation.

(1) Bond lengths determined by EXAFS agree closely with those from crystallography, there being a difference of ≤0.02 Å over all distances, including average M−S distances (Figures 2 and 3, Tables 1−3). Further, the bond variance parameters of ≤0.004 $Å^2$ over all distances are indicative of rigid dithiolene binding, as found for bdt complexes.[24]

(2) K-edge data indicate that the aromatic and aliphatic dithiolene ligands bdt and $S_2C_2Me_2$, respectively, are indistinguishable. Given that the latter and the pterin−dithiolene cofactor ligand are both dialkyldithiolenes, it follows that synthetic dithiolenes are accurate structural representations of the cofactor ligand in XAS experiments. Consequently, comparisons between synthetic complexes and protein sites are meaningful.

(3) The series of five-coordinate Mo^{IV} complexes **3**−**7** simulate protein ligation modes in three reduced active sites of the DMSOR family (Figure 1). Molybdenum K-edge shifts correlate with the electronegativity of the terminal ligands RQ^- (Q = O, S, Se) (Figure 4), and bond lengths follow the expected trend Mo−O < Mo−S < Mo−Se. Molybdenum XAS clearly distinguishes single O, S, and Se terminal ligations in the presence of four Mo−S(dithiolene) interactions.

(4) The six-coordinate M^{IV} complexes **8** and **11**−**13** are monocarbonyls with terminal thiolate or selenolate binding. As noted previously,[20,22] the stability of these complexes raises the possibility that analogously coordinated reduced enzyme sites could bind carbon monoxide. In this event, both edge (Figures 5−8) and EXAFS features (Figures 9−11) could distinguish CO-bound and five-coordinate sites. Elsewhere, we have argued that the shorter M−O bond in complexes with terminal RO^- ligands produces steric interactions between the R substituent and CO unfavorable to binding.[20,22]

(5) For selenolate complexes **7**, **8**, and **11**, M−Se bond distances determined by M and Se EXAFS are in satisfactory agreement (≤0.02 Å, Table 3), providing an internal check of the accuracy of the bond distances.

(6) Given the isostructural properties of molybdenum and tungsten complexes at parity of ligands and oxidation state, the distorted octahedral W^{VI} complex **14** is a plausible approximation (or better) of the oxidized monooxo sites of DMSOR. The one protein-bound site available for comparison, in the *R. sphaeroides* enzyme, is described as distorted trigonal prismatic with no sulfur ligand trans to the oxo ligand. The EXAFS data for **14** are fitted with two W−O distances differing by 0.27 Å and a single W−S distance differing by 0.01 Å from the average crystallographic distances. (The molybdenum analogue of **14** is unstable and has not been isolated.[23])

By including a larger set of variant terminal ligands, this study expands our previous XAS investigation[24] of bis(dithiolene)-molybdenum and -tungsten complexes which serve as symmetrized structural representations of enzyme active sites. Because of the internal consistency of EXAFS and X-ray crystallographic bond lengths, the full body of results should prove useful in characterizing and refining metric features and structures of enzyme sites. Current targets for XAS examinations include monodithiolene complexes, selenosulfido−thiolate ligands and their complexes, and M^{VI} species accessible by oxidative addition to bis(dithiolene)M(IV) complexes.

Acknowledgment. This research was supported by NSF Grant CHE 9423181 and NIH Grant RR-01209 (to K.O.H.) and by NSF Grant CHE 9876457 (to R.H.H.). The Stanford Synchrotron Radiation Laboratory is supported by the Department of Energy, Office of Basic Energy Sciences. The Structural Molecular Biology Program is supported by the National Institutes of Health, National Center for Research Resources, Biomedical Technology Program, and the DOE Office of Biological and Environmental Research. We thank Prof. H. Schindelin for access to ref 6 prior to publication.

Supporting Information Available: Figures S1−S8, showing normalized Mo and Se K-edge and W L_3-edge spectra and non-phase-corrected Fourier transforms of the complexes in Tables 2 and 3. This material is available free of charge via the Internet at http://pubs.acs.org.

IC000601R